J. Fluid Mech. (1987), *vol.* 178, *pp.* 221–241
Printed in Great Britain

Bragg scattering of surface waves by periodic bars: theory and experiment

By TETSU HARA

Department of Civil Engineering, University of Tokyo *and* Massachusetts Institute of Technology, Cambridge, MA 02139, USA

AND CHIANG C. MEI

Department of Civil Engineering, Massachusetts Institute of Technology, Cambridge, MA 02139, USA

(Received 11 June 1986)

We extend a recent linearized theory on Bragg scattering of surface waves by periodic sandbars to include second-order effects of the free surface and of the bars. New experiments are performed to verify the existence of the cutoff detuning frequency, the dispersive nature of the first-order wave envelope, and the radiation of second-order long waves. Measured transient and quasi-steady responses to incident wave packets and uniform wavetrains are compared with corresponding theoretical results. For quasi-steady incident waves of relatively small steepness it is found necessary to improve the theory to the second order in bar slope, in order that the calculated short-wave envelopes agree with those measured over the bars.

1. Introduction

Experiments by Heathershaw (1982) in a long wave tank have shown that abnormally large reflection can occur if the bottom is covered with sinusoidal bars whose length is half that of the incident waves. This phenomenon corresponds to Bragg scattering in other physical contexts and is due to the constructive interference of the reflected waves from each sandbar crest. Davies (1982) and Davies & Heathershaw (1984) have given a perturbation theory for the scattering by a finite number of parallel bars, but their theory is only valid away from resonance. A uniformly valid theory has been given by Mei (1985) which agrees reasonably well with Heathershaw's experiments at resonance.

In addition to the special case of precise resonance, there are several new features predicted by Mei which warrant experimental confirmation. Specifically, for small detuning, the envelopes of the first-order incident and/or reflected waves are found to be dispersive over long space and time scales. For uniform incident envelopes slightly detuned in frequency by Ω, there exists a cutoff frequency Ω_0 across which the behaviour of envelopes can be vastly different. Above cutoff, $\Omega^2 > \Omega_0^2$, the envelope is oscillating in x, and below cutoff, $\Omega^2 < \Omega_0^2$, it is monotonic in x. At the second order in wave slope, in addition to the usual long waves (set-down) that are locked to the envelopes of the first-order waves, there are also free long waves which propagate at the faster shallow-water wave speed. Since the variation of the short waves can be important to the formation of sand bars and the generation of long waves implies that bathymetry can alter the sea spectrum, it is worthwhile to seek experimental verification of these predictions.

One of the purposes of this paper is to describe new experiments which demonstrate these physical features. The second is to extend the second-order theory for the long waves. In our experiments with quasi-steady incident waves the amplitude of the bars was much greater than that of the waves. We have found it necessary to extend Mei (1985) to a higher order in order to improve the agreement between prediction and measurement.

2. The approximate equations

Starting from the linearized formulation for infinitesimal waves, Mei (1985) derived the evolution equations of the first-order envelopes. His reasoning for the second-order long waves was sketchy and results were incomplete. A more systematic nonlinear analysis is outlined here. Rigid bars are assumed.

In this problem there can be several small parameters: the wave slope kA, the mean bottom slope, the bar slope kD, the ratio of detuned frequency to wave frequency Ω/ω and the spatial modulation rate of the wave envelope. Although they can in principle be quite independent, the most general case is one in which they are all comparable. Therefore in this section we shall use ϵ to characterize all of them.

The velocity potential is governed by

$$\nabla^2\phi+\phi_{zz}=0 \tag{2.1}$$

in the fluid, where ∇ denotes the gradient operator in the horizontal plane (x,y). Combining the kinematic and dynamic conditions on the free surface and expanding about $z=0$, we get, up to third order in ϵ,

$$\begin{aligned}\phi_{tt}+g\phi_z=&\left\{-\tfrac{1}{2}[(\nabla\phi)^2+\phi_z^2]+\frac{1}{g}\phi_t\phi_{zt}\right\}_t-\nabla\cdot(\phi_t\nabla\phi)\\&+\left\{\frac{1}{2g}[\phi_t(\nabla\phi)^2+\phi_t\phi_z^2]_z-\frac{1}{g^2}\phi_t\phi_{zt}^2-\frac{1}{2g^2}\phi_{zzt}\phi_t^2\right\}_t\\&+\nabla\cdot\left\{-\tfrac{1}{2}\nabla\phi[(\nabla\phi)^2+\phi_z^2]+\frac{1}{g}\phi_t\phi_{zt}\nabla\phi+\frac{1}{2g}\phi_t^2\nabla\phi_z\right\}+O(\epsilon^4)\\&(z=0).\end{aligned} \tag{2.2}$$

Let h be the mean depth which varies slowly in x, and δ the upward deviation due to the bars which have scales comparable to those of the free surface. The kinematic condition at the sea bottom can be approximated to third order by

$$\nabla\phi\cdot\nabla h+\delta\nabla\phi_z\cdot\nabla h-\nabla\phi\cdot\nabla\delta-\delta\nabla\phi_z\cdot\nabla\delta+\phi_z+\delta\phi_{zz}+\tfrac{1}{2}\delta^2\phi_{zzz}=O(\epsilon^4)\quad(z=-h). \tag{2.3}$$

The free-surface displacement ζ is related to ϕ by the Bernoulli equation,

$$g\zeta+\zeta\phi_{tz}+\phi_t+\tfrac{1}{2}[(\nabla\phi)^2+\phi_z^2]=O(\epsilon^3)\quad(z=0). \tag{2.4}$$

All the bars are assumed to be parallel to the y-axis. At the edge of the bar field pressure and normal velocity must be continuous,

$$\{\phi_t+\tfrac{1}{2}[(\nabla\phi)^2+\phi_z^2]\}_-^+=0, \tag{2.5}$$

$$[\phi_x]_-^+=0. \tag{2.6}$$

Let us introduce the following:

$$x,y,z,t;\quad(x_1,y_1,t_1)\equiv\epsilon(x,y,t);\quad x_2,y_2,t_2\equiv\epsilon^2(x,y,t) \tag{2.7}$$

and expand ϕ and ζ as Fourier series,

$$\phi = \sum_{n=1} \epsilon^n \sum_{m=-n}^{n} \phi_{nm} \, \mathrm{e}^{-\mathrm{i}m\omega t}; \quad \zeta = \sum_{n=1} \epsilon^n \sum_{m=-n}^{n} \zeta_{nm} \, \mathrm{e}^{-\mathrm{i}m\omega t}, \tag{2.8}$$

where
$$\phi_{nm} = \phi^*_{n,-m}, \quad \zeta_{nm} = \zeta^*_{n,-m} \tag{2.9}$$

and
$$\phi_{nm} = \phi_{nm}(x, y, z; x_1, y_1, t_1; x_2, y_2, t_2); \quad \zeta_{nm} = \zeta_{nm}(x, y; x_1, y_1, t_1; x_2, y_2, t_2). \tag{2.10}$$

Assuming that the mean depth has straight and parallel contours, i.e. $h = h(x_1)$ and separating different orders and harmonics, we obtain at the leading order $O(\epsilon)$

$$\nabla^2\phi_{10} + \phi_{10zz} = 0 \quad (-h < z < 0), \tag{2.11}$$

$$\phi_{10z} = 0 \quad (z = 0), \tag{2.12}$$

$$\phi_{10z} = 0 \quad (z = -h) \tag{2.13}$$

for the slow oscillations, and

$$\nabla^2\phi_{11} + \phi_{11zz} = 0 \quad (-h < z < 0), \tag{2.14}$$

$$-\omega^2\phi_{11} + g\phi_{11z} = 0 \quad (z = 0), \tag{2.15}$$

$$\phi_{11z} = 0 \quad (z = -h) \tag{2.16}$$

for the fast oscillations. At the second order, we have

$$\nabla^2\phi_{20} + \phi_{20zz} = -(\nabla\cdot\nabla_1 + \nabla_1\cdot\nabla)\phi_{10} \quad (-h < z < 0), \tag{2.17}$$

$$\phi_{20z} = -\frac{\omega}{g}\nabla\cdot(\mathrm{i}\phi^*_{11}\nabla\phi_{11} + *) \quad (z = 0) \tag{2.18}$$

$$\phi_{20z} = -\nabla\phi_{10}\cdot(\nabla_1 h - \nabla\delta) + \delta\nabla^2\phi_{10} \quad (z = -h) \tag{2.19}$$

for the slow oscillations, and

$$\nabla^2\phi_{21} + \phi_{21zz} = -(\nabla\cdot\nabla_1 + \nabla_1\cdot\nabla)\phi_{11} \quad (-h < z < 0), \tag{2.20}$$

$$-\omega^2\phi_{21} + g\phi_{21z} = 2\mathrm{i}\omega\phi_{11t_1} \quad (z = 0), \tag{2.21}$$

$$\phi_{21z} = -\nabla\phi_{11}\cdot(\nabla_1 h - \nabla\delta) + \delta\nabla^2\phi_{11} \quad (z = -h) \tag{2.22}$$

for the fast oscillations.

From (2.11)–(2.13) the slow potential ϕ_{10} depends only on the slow variables

$$\phi_{10} = \phi_{10}(x_1, y_1, t_1; x_2, y_2, t_2) \tag{2.23}$$

and hence must represent long waves. The short waves can be solved by

$$\left.\begin{aligned} \phi_{11} &= (A\,\mathrm{e}^{\mathrm{i}S_+} + B\,\mathrm{e}^{\mathrm{i}S_-})f_0(z), \\ \zeta_{11} &= \tfrac{1}{2}(A\,\mathrm{e}^{\mathrm{i}S_+} + B\,\mathrm{e}^{\mathrm{i}S_-}), \end{aligned}\right\} \tag{2.24}$$

with
$$f_0 = -\frac{\mathrm{i}g}{2\omega}\frac{\cosh k(z+h)}{\cosh kh}, \tag{2.25}$$

$$S_\pm = \pm\frac{1}{\epsilon}\int^{x_1} \alpha(x_1)\,\mathrm{d}x_1 + \beta y, \tag{2.26}$$

$$\alpha = k\cos\theta, \quad \beta = k\sin\theta, \tag{2.27}$$

$$\omega^2 = gk\tanh kh, \tag{2.28}$$

where θ is the local inclination of the incident waves with respect to the x-axis. We now specify the bar profile by

$$\delta = \tfrac{1}{2}D(x_1, y_1)\left(\exp\frac{2\mathrm{i}}{\epsilon}\int^{x_1}\alpha(x_1)\,\mathrm{d}x_1 + *\right), \tag{2.29}$$

so that the Bragg resonance condition is met.

Solvability of the boundary-value problem for the second-order fast oscillations ϕ_{21} can be used to derive the governing equations for the first-order amplitudes A and B, with the results:

$$A_{t_1} + C_{\mathrm{g}}^{+}\cdot\nabla_1 A + \tfrac{1}{2}A\nabla_1\cdot C_{\mathrm{g}}^{+} = -\mathrm{i}\Omega_0 B\cos 2\theta, \tag{2.30a}$$

$$B_{t_1} + C_{\mathrm{g}}^{-}\cdot\nabla_1 B + \tfrac{1}{2}B\nabla_1\cdot C_{\mathrm{g}}^{-} = -\mathrm{i}\Omega_0 A\cos 2\theta, \tag{2.30b}$$

or equivalently,

$$\tfrac{1}{2}|A|^2_{t_1} + \tfrac{1}{2}\nabla_1\cdot(C_{\mathrm{g}}^{+}|A|^2) = -\frac{1}{2}\Omega_0 A^* B\cos 2\theta + *, \tag{2.31a}$$

$$\tfrac{1}{2}|B|^2_{t_1} + \tfrac{1}{2}\nabla_1\cdot(C_{\mathrm{g}}^{-}|B|^2) = +\frac{\mathrm{i}}{2}\Omega_0 A^* B\cos 2\theta + *, \tag{2.31b}$$

where

$$C_{\mathrm{g}}^{\pm} = (\pm\alpha, \beta)\frac{C_{\mathrm{g}}}{k}, \quad C_{\mathrm{g}} = \frac{\omega}{2k}\left(1 + \frac{2kh}{\sinh 2kh}\right) \tag{2.32}$$

and

$$\Omega_0 = \frac{\omega k D}{2\sinh 2kh} \tag{2.33}$$

is the cutoff frequency which couples A and B.

Let the nearly periodic bars be distributed within the domain $0 < x < L$ where kL is at least of the order ϵ^{-1}, as will be specified later. Continuity of pressure requires that

$$[\phi_{11}]^{+}_{-} = 0 \quad (x = 0, L), \tag{2.34}$$

while continuity of normal velocity requires that

$$[\phi_{11x}]^{+}_{-} = 0 \quad (x = 0, L), \tag{2.35}$$

$$[\phi_{10x}]^{+}_{-} = 0 \quad (x = 0, L). \tag{2.36}$$

Because of (2.34) and (2.35) we have

$$[A]^{+}_{-} = 0, \quad [B]^{+}_{-} = 0 \quad (x = 0, L) \tag{2.37a, b}$$

Using these results the right-hand sides of (2.17)–(2.19) vanish and the second-order slow potential ϕ_{20} satisfies the same homogenous equations (2.11)–(2.13) as ϕ_{10}. Hence ϕ_{20} depends only on the slow coordinates also, i.e.

$$\phi_{20} = \phi_{20}(x_1, y_1, t_1; x_2, y_2, t_2). \tag{2.38}$$

So far these results have been derived and discussed by Mei (1985).

At the third order the slow oscillations are governed by

$$\nabla^2\phi_{30} + \phi_{30zz} = -\nabla_1^2\phi_{10} \quad (-h < z < 0) \tag{2.39}$$

in the fluid,

$$\phi_{30z} = -\frac{1}{g}\phi_{10t_1t_1} + \frac{1}{g}\Big[-|\nabla\phi_{11}|^2 - |\phi_{11z}|^2 + \frac{\omega^2}{g}(\phi_{11}\phi_{11z}^*) + *\Big]_{t_1}$$
$$-\frac{\omega}{g}[\nabla_1\cdot(\mathrm{i}\phi_{11}^*\nabla\phi_{11} + *) + \nabla\cdot(\mathrm{i}\phi_{11}^*\nabla_1\phi_{11} + *)]$$
$$-\frac{\omega}{g}\nabla\cdot(\mathrm{i}\phi_{11}^*\nabla\phi_{21} + * + \mathrm{i}\phi_{21}^*\nabla\phi_{11} + *) - \frac{1}{g}\nabla\cdot(\phi_{11t_1}^*\nabla\phi_{11} + *) \quad (z = 0) \tag{2.40}$$

on the free surface, and

$$\phi_{30z} = -\nabla_1\phi_{10}\cdot(\nabla_1 h - \nabla\delta) \quad (z = -h) \tag{2.41}$$

on the bottom. Integrating (2.39) with respect to z from $-h$ to 0, using the boundary conditions, and averaging over the horizontal coordinates on the short scale, we obtain, owing to the spatial periodicity on the short scale,

$$\phi_{10t_1t_1} - g\nabla_1\cdot(h\nabla_1\phi_{10}) = -\nabla_1\cdot(\mathrm{i}\omega\overline{\phi_{11}^*\nabla\phi_{11}} + *)$$
$$-\overline{(|\nabla\phi_{11}|^2 + |\phi_{11z}|^2)}_{t_1} + \frac{\omega^2}{g}\overline{(\phi_{11}\phi_{11z}^* + *)}_{t_1} \quad (z = 0), \tag{2.42}$$

where overbars denote averages over a periodic domain in the (x, y)-plane. Equation (2.42) is a shallow-water equation governing the long-wave potential ϕ_{10}.

From the spatial average of the Bernoulli equation we find the second-order mean sea level

$$\bar{\zeta}_{20} = \frac{\omega^2}{g^2}\overline{(\phi_{11}\phi_{11z}^* + *)} - \frac{1}{g}\phi_{10t_1} - \frac{1}{g}\overline{(|\nabla\phi_{11}|^2 + |\phi_{11z}|^2)} \quad (z = 0). \tag{2.43}$$

This can be used to obtain an equation for $\bar{\zeta}_{20}$ from (2.42):

$$\bar{\zeta}_{20t_1t_1} - g\nabla_1\cdot(h\nabla_1\bar{\zeta}_{20}) = -g\nabla_1\cdot\Big\{h\nabla_1\Big[\frac{\omega^2}{g^2}\overline{(\phi_{11}\phi_{11z}^* + *)}$$
$$-\frac{1}{g}\overline{(|\nabla\phi_{11}|^2 + |\phi_{11z}|^2)}\Big]\Big\} + \frac{\omega}{g}\nabla_1\cdot\overline{(\mathrm{i}\phi_{11}^*\nabla\phi_{11} + *)}_{t_1} \quad (z = 0) \tag{2.44}$$

Introducing (2.24) into (2.43) and (2.44) we obtain the following:

$$\bar{\zeta}_{20} = -\frac{1}{g}\phi_{10t_1} - \frac{k}{2\sinh 2kh}(|A|^2 + |B|^2) \tag{2.45}$$

and

$$\bar{\zeta}_{20t_1t_1} - g\nabla_1\cdot(h\nabla_1\bar{\zeta}_{20}) = g\nabla_1\cdot\Big\{h\nabla_1\Big[\frac{k}{2\sinh 2kh}(|A|^2 + |B|^2)\Big]\Big\}$$
$$-\frac{g}{2\omega}\{\alpha(|A|^2 - |B|^2)_{x_1} + \beta(|A|^2 + |B|^2)_{y_1}\}_{t_1}. \tag{2.46}$$

Along the boundaries of the bar field, continuity of pressure and normal velocity requires at $O(\epsilon^2)$ that

$$[\phi_{10t_1} + |\nabla\phi_{11}|^2 + |\phi_{11z}|^2]^+_- = 0 \tag{2.47}$$
$$[\phi_{10x_1} + \phi_{20x}]^+_- = 0 \quad (x = 0, L). \tag{2.48}$$

Because of (2.37) the quadratic terms in (2.47) are continuous, implying,

$$[\phi_{10}]^+_- = 0 \quad (x = 0, L) \tag{2.49}$$

and, because of (2.38), $$[\phi_{10x_1}]^+_- = 0 \quad (x = 0, L). \tag{2.50}$$

The boundary conditions along the edge of the bar field are, from (2.49, 2.50) and (2.45),

$$[\bar{\zeta}_{20}]^+_- = 0 \quad (x = 0, L), \tag{2.51}$$

$$[\bar{\zeta}_{20x_1}]^+_- = -\frac{k}{2\sinh 2kh}[(|A|^2+|B|^2)_{x_1}]^+_- \quad (x = 0, L). \tag{2.52}$$

We summarize the key results for the special case of constant mean depth and normal incidence $\partial/\partial y = \partial/\partial y_1 = 0$. Equations (2.30$a, b$) become simply

$$A_{t_1} + C_g A_{x_1} = -i\Omega_0 B, \quad B_{t_1} - C_g B_{x_1} = -i\Omega_0 A. \tag{2.53a, b}$$

Also, subtraction of (2.31b) from (2.31a) gives

$$\tfrac{1}{2}C_g(|A|^2+|B|^2)_{x_1} + \tfrac{1}{2}(|A|^2-|B|^2)_{t_1} = -i\Omega_0 A^*B + *, \tag{2.54}$$

which can be used to rewrite (2.46):

$$\bar{\zeta}_{20t_1t_1} - gh\bar{\zeta}_{20x_1x_1} = \frac{1}{\rho}\mathscr{S}_{x_1x_1} + \frac{g\Omega_0}{C}(iA^*B + *)_{x_1}, \tag{2.55}$$

where $\mathscr{S}$ is the radiation stress due to right- and left-going waves

$$\mathscr{S} = \tfrac{1}{2}\rho g\left(\frac{2C_g}{C} - \frac{1}{2}\right)(|A|^2+|B|^2). \tag{2.56}$$

In Mei (1985), (2.55) was stated with only the radiation stress term on the right-hand side, and was therefore incomplete.

These equations are valid for $(kx_1, ky_1, \omega t_1) = O(1)$.

3. Numerical procedure for transient scattering of a wave packet by bars on constant mean depth

To gain some physical insight we shall first consider a finite stretch of bars with constant amplitude D, superimposed on a constant mean depth. A packet of short waves is incident normally from $x_1 < 0$ towards the bars within $0 < x_1 < L_1$, where $L_1 = \epsilon L = O(1)$. Equations (2.53a, b) can be combined to give a Klein–Gordon equation which is formally solvable by Fourier transform for any initial condition. Explicit evaluation of the inverse transform is however not always easy unless further restrictions are imposed. We therefore apply the numerical method of finite differences as follows. First there is no more need to distinguish x_1 from x, t_1 from t, etc. Let the dimensionless variables

$$x' = \frac{x}{L}, \quad t' = \frac{tC_g}{L}, \quad (A', B') = \frac{(A, B)}{A_m} \tag{3.1}$$

be introduced, where A_m is the maximum amplitude of the incident waves. Then (2.53a, b) become, after dropping primes for brevity,

$$A_t + A_x = -i\sigma B, \tag{3.2}$$

$$B_t - B_x = -i\sigma A, \tag{3.3}$$

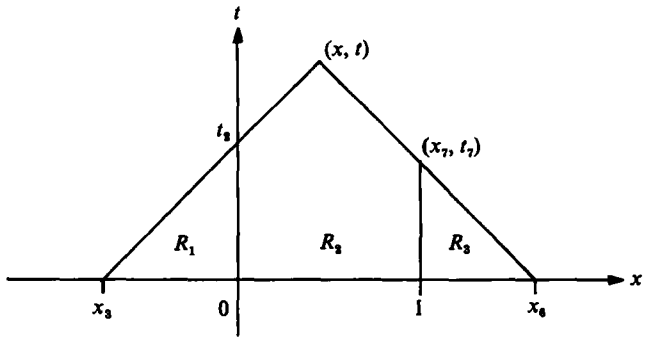

FIGURE 1. The characteristic triangle.

where
$$\sigma = \frac{\Omega_0 L}{C_g}. \tag{3.4}$$

We use the third-order Adams–Bashforth finite-difference scheme and discretize (3.2) as

$$\frac{A_j^{n+1}-A_j^n}{\Delta t}+\frac{1}{2\Delta x}[\tfrac{23}{12}(A_{j+1}^n-A_{j-1}^n)-\tfrac{16}{12}(A_{j+1}^{n-1}-A_{j-1}^{n-1}) + \tfrac{5}{12}(A_{j+1}^{n-2}-A_{j-1}^{n-2})] = -i\sigma[\tfrac{23}{12}B_j^n-\tfrac{16}{12}B_j^{n-1}+\tfrac{5}{12}B_j^{n-2}], \tag{3.5}$$

where the superscripts refer to the time-step and the subscripts to the steps along x. The barred region $0 < x < 1$ is divided into N intervals with $j = 0$ at $x = 0$ and $j = N$ at $x = 1$. Equation (3.3) is discretized similarly by interchanging A and B. This scheme has an error of $O(\Delta x^2, \Delta t^3)$ and is absolutely stable if $\Delta t/\Delta x < 0.75$.

The known boundary values at the edges are

$$A = A(t) \quad (x = 0), \tag{3.6}$$

$$B = 0 \quad (x = 1). \tag{3.7}$$

From (3.2) and (3.3) we can also infer the boundary values of A at $x = 1$ ($j = N$) in terms of A_x and B, and B at $x = 0$ ($j = 0$) in terms of B_x and A. In the discretized form the value of B_0^{n+1} is given by

$$\frac{B_0^{n+1}-B_0^n}{\Delta t}-\frac{1}{2\Delta x}[\tfrac{23}{12}(-3B_0^n+4B_1^n-B_2^n)-\tfrac{16}{12}(-3B_0^{n-1}+4B_1^{n-1}-B_2^{n-1}) + \tfrac{5}{12}(-3B_0^{n-2}+4B_1^{n-2}-B_2^{n-2})] = -i\sigma[\tfrac{23}{12}A_0^n-\tfrac{16}{12}A_0^{n-1}+\tfrac{5}{12}A_0^{n-2}]. \tag{3.8}$$

For the second-order long waves we define the normalized mean free surface by

$$\zeta' = \bar{\zeta}_{20}/kA_m^2. \tag{3.9}$$

Equation (2.55) reduces to

$$\zeta_{tt}-C_0^2\zeta_{xx} = \left(\frac{C_g}{C}-\frac{1}{4}\right)\frac{g}{kC_g^2}(|A|^2+|B|^2)_{xx}+\frac{g\sigma}{kCC_g}(iA^*B+*)_x, \tag{3.10}$$

$$C_0 = (gh)^{\frac{1}{2}}/C_g. \tag{3.11}$$

The Riemann method for obtaining the usual d'Alembert's solution for the one-dimensional wave equation can be modified here to account for the jump conditions

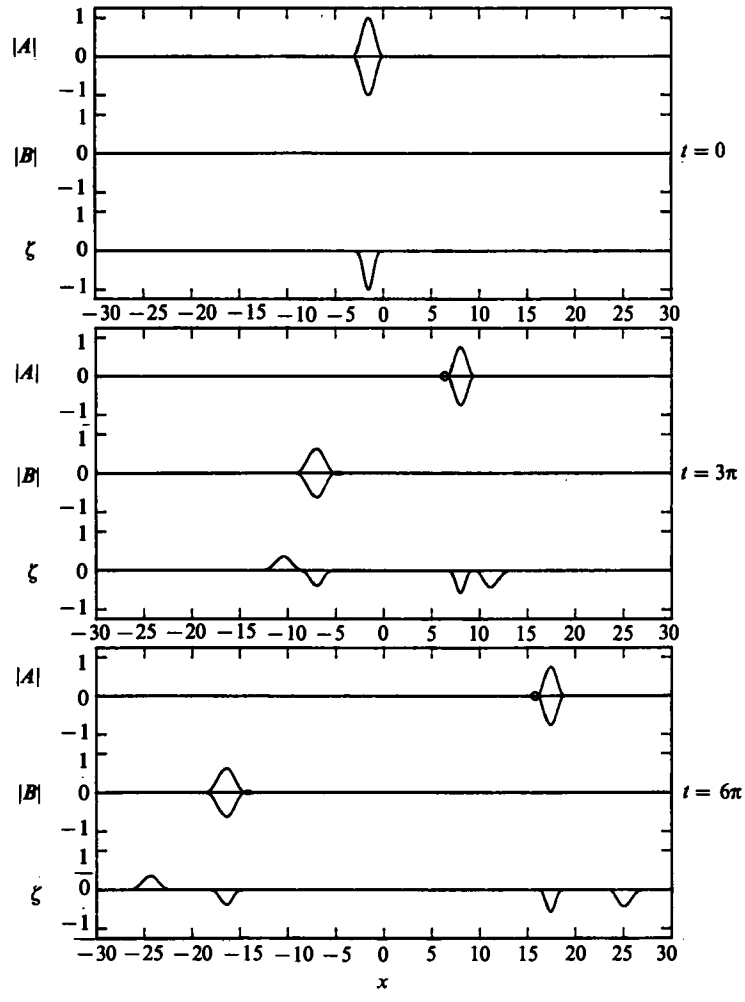

FIGURE 2. Incident and reflected wave amplitudes and second-order long waves ($\sigma = 1.0$).

at the edges of the bar regions. The solution depends on the location of the observer in the (x, t)-plane. Referring to figure 1, if the characteristic triangle defining the domain of dependence intersects all three regions, the solution is

$$\zeta(x,t) = \frac{1}{2C_0}\sum_{i=1}^{3}\iint_{R_i} h_i\,\mathrm{d}x\,\mathrm{d}t + \frac{1}{2C_0}\int_{x_3}^{x_6}\zeta_t(x,0)\,\mathrm{d}x + \tfrac{1}{2}[\zeta(x_3,0)+\zeta(x_6,0)] - \frac{C_0}{2}\int_0^{t_2}[\zeta_x(0,t)]^{\pm}_{-}\,\mathrm{d}t - \frac{C_0}{2}\int_0^{t_7}[\zeta_x(1,t)]^{\pm}_{-}\,\mathrm{d}t, \quad (3.12)$$

where R_1, R_2 and R_3 are defined in figure 1, within which the forcing functions are

$$\begin{pmatrix} h_1 \\ h_2 \\ h_3 \end{pmatrix} = \left(\frac{C_g}{C} - \frac{1}{4}\right)\frac{g}{kC_g^2}\begin{pmatrix} (|A|^2+|B|^2)_{xx} \\ (|A|^2+|B|^2)_{xx} \\ |A|^2_{xx} \end{pmatrix} + \frac{g\sigma}{kCC_g}\begin{pmatrix} 0 \\ (\mathrm{i}A^*B+*)_x \\ 0 \end{pmatrix}. \quad (3.13)$$

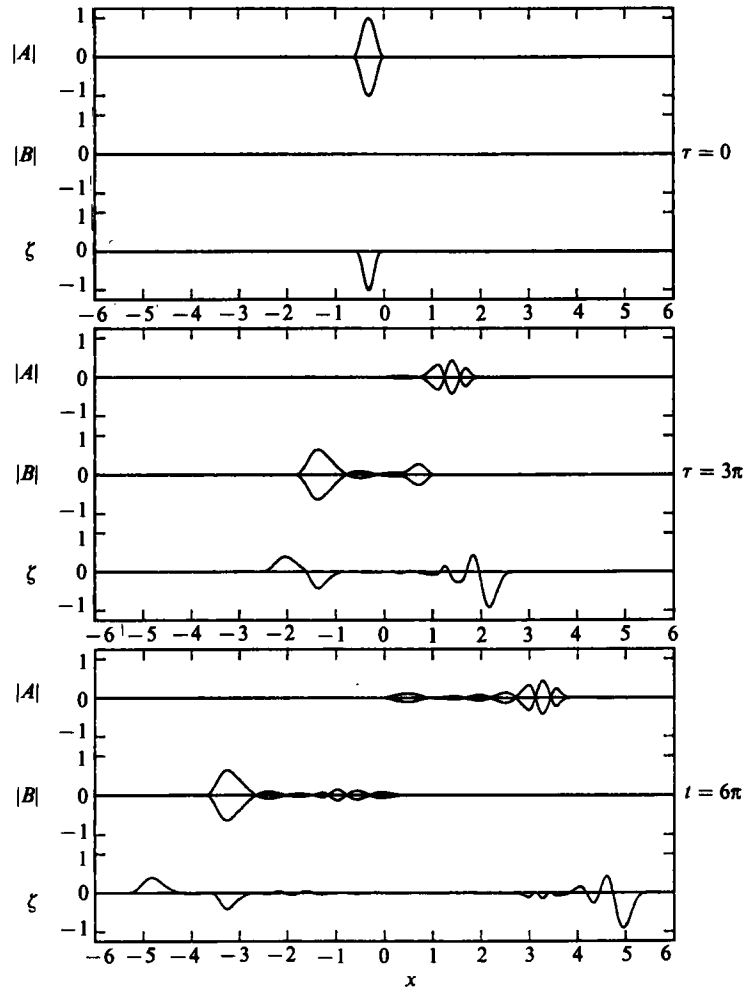

FIGURE 3. Incident and reflected wave amplitudes and second-order long waves ($\sigma = 5.0$).

Initially the incident wave packet is to the left of the bar field, hence the long wave consists only of the locked set-down,

$$\zeta(x,t) = \zeta(t-x) = \frac{g|A|^2}{k(C_g^2-gh)}\left(\frac{C_g}{C}-\frac{1}{4}\right). \tag{3.14}$$

The initial value of ζ_t needed in (3.12) can be derived by differentiation.

As an example consider the following incident wave packet:

$$\left.\begin{aligned} A &= \sin^2(t-x) \quad (t-x\in(0,\pi)),\\ A &= 0 \qquad\qquad (t-x\notin(0,\pi)),\end{aligned}\right\} \tag{3.15}$$

and $kh = 1$. At $t = 0$, the leading edge of the incident group arrives at the left edge of the bar field at $x = 0$. The first-order scattering is illustrated in figures 2 and 3 with the dimensionless bar-field width σ as the parameter. Even for small $\sigma(=1)$,

reflection is significant. Because of dispersion, the right-going envelope splits into two before escaping to the barless region $x > 1$ (figure 2). For a much longer L with $\sigma = 5$ and the same incident envelope, now given by $\sin^2 5(t-x)$ because of the normalization, not only is the reflected envelope much greater than the transmitted envelope, but group splitting becomes more prominent with the birth of many new and smaller groups propagating in both directions (figure 3).

Finally we also plot in figures 2 and 3 the evolution of long waves for the input (3.14). Note that the faster long waves propagating at the speed $(gh)^{\frac{1}{2}}$ finally run away from the slower long waves locked to the wave envelopes. For still greater σ, it is possible to have very little transmission of the short waves, but the radiated long waves advancing to $x \to +\infty$ at $(gh)^{\frac{1}{2}}$ can still be significant.

4. Comparison of experiments and theory for transient scattering in a tank of finite length

Measurements were carried out in a glass-walled wave tank of dimensions 21.82 m × 38.3 cm (width) × 60 cm (depth). The wavy bed was in the region $0 < x < 12$ m and consisted of 20 periods of sinusoidal waves of wavelength 60 cm and amplitude 2.91 cm. The water depth was kept at 14.8 cm or 20.0 cm. The bed waves were constructed by bending Plexiglas sheets of 0.3175 cm thickness on a contoured wooden frame which was glued to the tank bottom. A horizontal shelf (-6.1 m $< x < 0$) and a plane slope (-7.32 m $< x < -6.10$ m) provided transition from the mean height of 5.40 cm to the original tank bottom near the wavemaker (at $x = -9.09$ m). A vertical endwall was fixed at the far end at $x = 12.0$ m, which coincided with the nodal line of the bar wave. See figure 4.

By a programmable piston wavemaker, a wave packet of finite duration

$$\left.\begin{aligned} A &= A_{\mathrm{m}} \sin^2 \Omega\left(t - \frac{(x+x_{\mathrm{c}})}{C_{\mathrm{g}}}\right), \quad \Omega\left[t - \frac{(x+x_{\mathrm{c}})}{C_{\mathrm{g}}}\right] \in (0, \pi) \\ &= 0, \qquad\qquad\qquad\qquad \Omega\left[\tau - \frac{(x+x_{\mathrm{c}})}{C_{\mathrm{g}}}\right] \notin (0, \pi), \end{aligned}\right\} \tag{4.1}$$

were generated, where $-x_{\mathrm{c}}$ was the leading edge of the packet at $t = 0$. The typical wave amplitude ranged from 1.45 to 2.0 cm and hence was comparable with that of the bars, in accordance with the theoretical assumption. The main goal was to check the dispersive effects of group splitting at the first order and the associated second-order long waves. The surface-water elevation was measured by capacitance-type wave gauges. The finite packet duration enabled us to concentrate on the evolution involving only one reflection from the far end; recording was terminated before reflection from the wavemaker was felt. Measurements were first made in the tank before installing the bars. Records were taken near the mid-length of the tank for 66 s, the first 5 s of which were averaged to obtain the mean water level. A fast Fourier transform was then used to separate the second-order long waves within the band 0–0.25 Hz and the short waves within the band 0.25–1.4 Hz. The maximum amplitude A_{m} was small enough that the sideband instability was not significant. Because of the long distance of propagation there were some effects of dispersion and dissipation, resulting in slight flattening of the envelope.

With the bars, wave records were taken at $x = -x_{\mathrm{c}} = -6.0$ m, which were used as the initial conditions. Near three other stations: $x = 0$ m, 6.0 m, and 12.0 m records were taken at 5 cm intervals along the tank for about 10 points for two purposes.

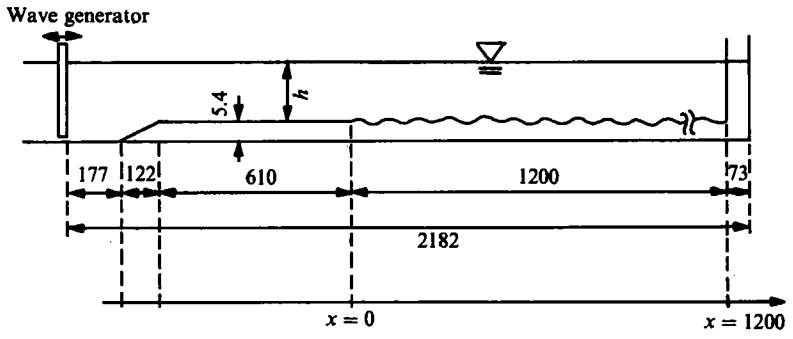

FIGURE 4. Experimental set-up. Units are in cm.

First, the wave records at two stations separated by $\frac{1}{4}$ wavelength (30 cm) were used to separate incident and reflected short waves. Secondly, the measured long waves obtained by fast Fourier transform correspond to the total ζ_{20} in the theory. This ζ_{20} consists of two components:

$$\zeta_{20} = \bar{\zeta}_{20} + \zeta'_{20},$$

where $\bar{\zeta}_{20}$ is the spatial average of ζ_{20}, and ζ'_{20} is the component which changes slowly in time but oscillates fast in space. Since only $\bar{\zeta}_{20}$ is calculated in the theory, we have to separate ζ'_{20} from the measured ζ_{20} before comparing the experimental results with the theoretical simulations. It can be shown that

$$\zeta'_{20} = \frac{k}{2\sinh 2kh}(1+2\sinh^2 kh)(AB^* \mathrm{e}^{2\mathrm{i}S_+} + *), \tag{4.2}$$

which depends on local A and B, and is zero midway between a node and its adjacent antinode. Therefore we first determined the nodes and the antinodes from the 5 cm interval records, then selected the measurement point where ζ'_{20} is nearly zero ($x = -0.15$ m, 5.80 m, 11.85 m). The long-wave records obtained at those points were compared with the simulations.

With bars spanning $0 < x < 12$ m we tested incident packets of the form (4.1) with a variety of parameters. We only display in figure 5 the records for one typical case which shows the incident and the reflected waves clearly. For this case $h = 14.8$ cm, $\omega = 5.77\ \mathrm{s}^{-1}$, $\Omega_0 = 0.196\ \mathrm{s}^{-1}$, $\Omega/\Omega_0 = 1$, and $A_\mathrm{m} = 1.48$ cm. At the mid-length of the bar region ($x = 6.0$ m), splitting into groups is evident, indicating the effect of envelope dispersion. At the endwall, $x = 12.0$ m, group splitting is again prominent.

To obtain the theoretical envelopes of the first-order waves (A and B), we imposed the boundary condition at the vertical endwall at $x = 12.0$ m:

$$\phi_{11x} = 0 \quad \text{at } x = 12.0 \text{ m}. \tag{4.3}$$

It is important that the wall coincides with the last node of the bars so that

$$\zeta = D\sin 2kx = \tfrac{1}{2}D[\exp(2\mathrm{i}kx - \mathrm{i}\tfrac{1}{2}\pi) + *]. \tag{4.4}$$

It follows from (2.26) and (2.29) that

$$S_\pm = \pm(kx - \tfrac{1}{4}\pi) \tag{4.5}$$

so that

$$A = \mathrm{i}B \quad \text{at } x = L = 12 \text{ m}. \tag{4.6}$$

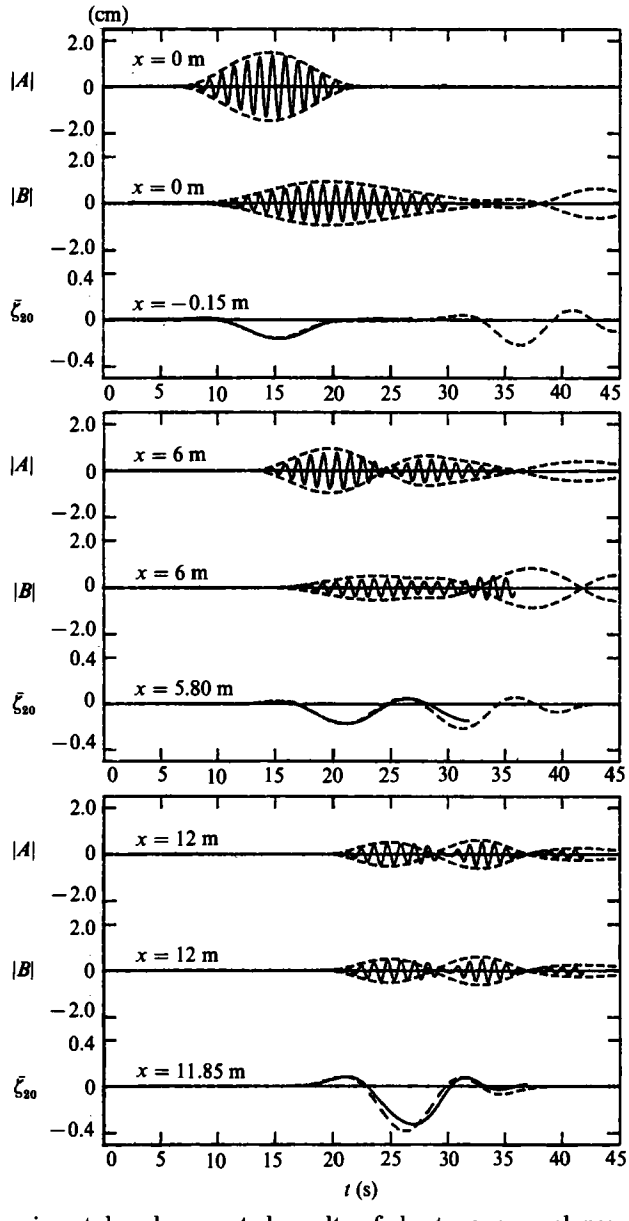

FIGURE 5. Experimental and computed results of short-wave envelopes and long waves: ----, computed results; ——, measured waves. The ends of the plotted wave records indicate the termination of recording.

With this boundary condition we calculated the envelopes of the first-order waves (A and B). After normalizing by the measured amplitude at $x = -x_c$ the result is plotted in figure 5 for comparison; the discrepancy between theory and measurements is small and is due in part to viscous dissipation. An attenuation factor $\exp(-k_1 X)$ can be defined where X is the distance, and

$$k_1 = \frac{k}{\sqrt{2}b}\left(\frac{\nu}{\omega}\right)^{\frac{1}{2}}\left(\frac{2kb+\sinh 2kh}{2kh+\sinh 2kh}\right) \tag{4.7}$$

(Hunt 1952) is the spatial damping rate, $2b$ is the width of the wave tank, and ν is the viscosity of water. In our experiment, the value of k_1 is 9.02×10^{-3} m^{-1}. Since the distance between the initial point of measurement and the endwall is 18 m, the attenuation factor is approximately $e^{-k_1 X} = 0.85$, which is consistent with the slight discrepancy seen in figure 5.

The set-down long waves locked to the incident group can be readily seen in the record at $x = 0$ m. The record at $x = 6$ m shows an elevation slightly ahead of the short waves, signalling the faster speed of the free long waves. Although the amplitude of the transmitted short waves is reduced to one-third of its original value, the long wave keeps its magnitude throughout the bar region. Near the endwall ($x = 11.85$ m) the long-wave amplitude is doubled owing to reflection. To simulate the experiment theoretically we impose at the vertical endwall the boundary condition

$$\phi_{10x_1} = 0 \quad \text{at } x = 12 \text{ m}, \tag{4.8}$$

which implies, by virtue of (2.45) and (4.6),

$$\bar{\zeta}_{20x_1} = \frac{\Omega_0}{C_g}\frac{2k|A|^2}{\sinh 2kh}. \tag{4.9}$$

Owing to second-order effects in the kinematic condition at the wavemaker and to the change of depth between the wavemaker and the bars, the long wave measured at $x = -6.0$ m is slightly reduced from the intended value (3.14) by a factor γ which varied with tests. In the case of figure 5, γ is found empirically to be 0.64. This discrepancy must imply the existence of a free long wave propagating from $x = -6.0$ m towards the bars at the speed $(gh)^{\frac{1}{2}}$. In our theoretical simulation we added to the locked long wave the free wave $\bar{\zeta}_f$, which is the homogeneous solution to (2.55) subject to the boundary conditions

$$\bar{\zeta}_{fx_1} = 0 \quad \text{for all } t > 0, \quad \text{at } x = 12.0 \text{ m} \tag{4.10}$$

and

$$\left.\begin{matrix}\zeta_f = (\gamma-1)\bar{\zeta}_{20} \\ = 0\end{matrix}\right\} = \frac{g(\gamma-1)}{C_g^2-gh}\left(\frac{C_g}{C}-\frac{1}{4}\right)|A_m|^2\sin^4\Omega t \quad \left.\begin{matrix}(\Omega t\in(0,\pi))\\(\Omega t\notin(0,\pi))\end{matrix}\right\} \quad \text{at } x = -6.0 \text{ m}. \tag{4.11}$$

The solution is

$$\bar{\zeta}_f = \bar{\zeta}_{f1} + \bar{\zeta}_{f2},$$

where

$$\left.\begin{aligned}\bar{\zeta}_{f1} &= \frac{g(\gamma-1)}{C_g^2-gh}\left(\frac{C_g}{C}-\frac{1}{4}\right)|A_m|^2\sin^4\left[\Omega t-\frac{x+6}{(gh)^{\frac{1}{2}}}\right] && \left(\Omega t-\frac{x+6}{(gh)^{\frac{1}{2}}}\in(0,\pi)\right),\\ \bar{\zeta}_{f1} &= 0 && \left(\Omega t-\frac{x+6}{(gh)^{\frac{1}{2}}}\notin(0,\pi)\right),\end{aligned}\right\}$$

and

$$\left.\begin{aligned}\bar{\zeta}_{f2} &= \frac{g(\gamma-1)}{C_g^2-gh}\left(\frac{C_g}{C}-\frac{1}{4}\right)|A_m|^2\sin^4\left[\Omega t+\frac{x-30}{(gh)^{\frac{1}{2}}}\right] && \left(\Omega t+\frac{x-30}{(gh)^{\frac{1}{2}}}\in(0,\pi)\right),\\ \bar{\zeta}_{f2} &= 0 && \left(\Omega t+\frac{x-30}{(gh)^{\frac{1}{2}}}\notin(0,\pi)\right).\end{aligned}\right\} \tag{4.12}$$

In these formulas we have written x, t for x_1, t_1. The resulting long wave $\bar{\zeta}_f + \bar{\zeta}_{20}$ is compared to the measurement; again the agreement is quite satisfactory.

For all other tests with slightly different ω, Ω and h, similar agreement has been

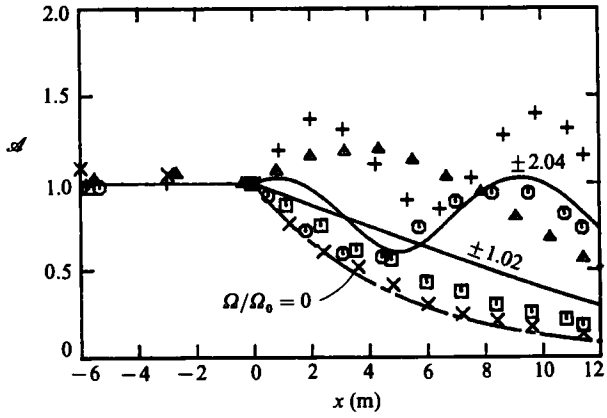

FIGURE 6. Wave height distribution at antinodes: +, $\Omega/\Omega_0 = 2.04$; △, 1.02; ×, 0; □, −1.02; ○, −2.04. Theoretical solutions are shown by curves: numbers by the curves give Ω/Ω_0.

found; further details are given in Hara (1985). We can therefore conclude that the simple asymptotic theory correctly predicts the dispersive nature of the envelope and the associated long waves within the stated realm of validity.

5. Experiments for steady incident waves

In order to verify that the bars give rise to the cutoff frequency Ω_0 across which the behaviour of the first-order envelope changes qualitatively, the second part of our experiments is for steady incident wavetrains within a narrow band of the Bragg resonance frequency, i.e. $A = A_m \exp i\Omega(x/C_g - t)$. Both positive ($\Omega > 0$) and negative ($\Omega < 0$) detuning were tested. Using the same bars as described in §4, we also located the vertical endwall at two different stations: $x = 6.0$ m and 12.0 m. Two mean water depths were used: 14.8 cm and 20.0 cm.

For steady waves, reflection from both the endwall and the wavemaker is important. If the incident wave amplitude is moderately large, the second-order long wave and sideband instability can be appreciable, and affected by the changing depth near the wavemaker. To avoid these complications we chose to reduce the incident wave amplitude A_m to the range of 0.164–0.735 cm, considerably less than that for the wave-packet experiments. Owing to complete reflection at the endwall, there were standing waves in the whole tank. At the antinodes the wave amplitude is given by $|A| + |B|$. A wave gauge was moved along the tank at 1 cm intervals to locate the antinodes. At each antinode, time records of 30 wave periods were used to get an average amplitude. The data so obtained are normalized by the amplitude of the free surface at the antinode just outside the bar region (near $x = 0$ m) and are plotted in figure 6. The range of input data relevant to figure 6 is given in table 1.

All the measured envelopes display the qualitative behaviour predicted by the first-order theory of Mei. In particular, when $|\Omega/\Omega_0| < 1$ the envelope decays monotonically in x away from the incident edge. For $|\Omega/\Omega_0|$ exceeding 1, the envelope becomes increasingly oscillatory in x. These data are first compared with calculations according to the first-order theory governed by (2.53a, b), subject to the boundary conditions (4.6) and (2.37a, b). The results can be obtained from (6.22) by letting $\alpha_2 = 0$.

For $(\Omega/\Omega_0)^2 < 1$ agreement between theory and experiment is fair, as shown in

Case	Ω/Ω_0	$\lvert A_m\rvert$ (cm)
1	2.04	0.165
2	1.02	0.164
3	0	0.203
4	−1.02	0.735
5	−2.04	0.232

TABLE 1. Parameters of steady incident waves: $L = 12.0$ m; $h = 14.8$ cm; $\omega = 5.77\ \mathrm{s}^{-1}$; $\Omega_0 = 0.196\ \mathrm{s}^{-1}$

figure 6. But for $(\Omega/\Omega_0)^2 = 1$ and > 1 there is little agreement; in the latter case the envelope is highly oscillatory. Also in the theory the envelope should be even in Ω, but the measured data clearly are different for positive and negative detuning. These discrepancies suggest the need for a better approximation which includes higher x-derivatives whose importance accumulates with distance. Since kA (≈ 0.02) is much less than kD (≈ 0.15) it is reasonable to ignore nonlinearity on the free surface. This amounts to using two small parameters $\mu = O(kA)$ and $\epsilon = O(kD)$ with $\mu \ll \epsilon$. The higher-order theory involves lengthy algebra, and will be carried out in the next section only to the extent needed for the present problem. Specifically we restrict to two dimensions x and z, constant mean depth and infinitesimal waves.

6. Simulation of experiments for steady waves by a higher-order theory

We first consider the general case $(\Omega/\Omega_0)^2 \neq 1$. The total width L is assumed to be so long that $\epsilon kL \gg 1$. With the linearized conditions on the free surface it is only necessary to assume

$$\phi = (\phi_{11} + \epsilon\phi_{21} + \epsilon^2\phi_{31} + \ldots)\, \mathrm{e}^{-\mathrm{i}\omega t} + *. \tag{6.1}$$

We now need the explicit solution of ϕ_{11} and ϕ_{21} in order to examine the solvability of ϕ_{31}.

The solution can be written:

$$\phi_{21} = \phi_{21}^{+1}\, \mathrm{e}^{\mathrm{i}S_+} + \phi_{21}^{-1}\, \mathrm{e}^{\mathrm{i}S_-} + \phi_{21}^{+3}\, \mathrm{e}^{3\mathrm{i}S_+} + \phi_{21}^{-3}\, \mathrm{e}^{3\mathrm{i}S_-}, \tag{6.2}$$

where the first harmonic is

$$\phi_{21}^{\pm 1} = \mp \frac{g}{2\omega k} \frac{Q \sinh Q}{\cosh kh} \begin{pmatrix} A \\ B \end{pmatrix}_{x_1} - \frac{\mathrm{i}gkD}{4\omega} \frac{\sinh Q}{\cosh kh} \begin{pmatrix} B \\ A \end{pmatrix}, \tag{6.3}$$

with $Q = k(z+h)$. This third harmonic $\phi_{21}^{\pm 3}$ satisfies

$$f_{zz} - (3k)^2 f = 0 \quad (-h < z < 0), \tag{6.4}$$

$$-\omega^2 f + g f_z = 0 \quad (z = 0), \tag{6.5}$$

$$f_z = -\tfrac{3}{2}k^2 D \phi_{11}^{\pm 1} \quad (z = -h), \tag{6.6}$$

where $\phi_{21}^{\pm 3}$ is denoted by f for brevity. The solution is

$$\phi_{21}^{\pm 3} = \frac{\mathrm{i}\omega D}{4 \sinh kh} \begin{pmatrix} A \\ B \end{pmatrix} \left[\sinh 3Q - \frac{\cosh 4kh + 2\cosh 2kh}{\sinh 4kh + 2 \sinh 2kh} \cosh 3Q \right]. \tag{6.7}$$

At the third order we only need the governing equations for the first harmonic $\phi_{31}^{\pm 1}$:

$$f_{zz}-k^2 f = \mp 2ik\phi_{11x_2}^{\pm 1} \mp 2ik\phi_{21x_1}^{\pm 1} - \phi_{11x_1x_1}^{\pm 1} \quad (-h < z < 0), \tag{6.8}$$

$$-\omega^2 f + g f_z = 2i\omega\phi_{11t_2}^{\pm 1} + 2i\omega\phi_{21t_1}^{\pm 1} - \phi_{11t_1t_1}^{\pm 1} \quad (z = 0), \tag{6.9}$$

$$f_z = \tfrac{1}{2}k^2 D\phi_{21}^{\mp 1} - \tfrac{3}{2}k^2 D\phi_{21}^{\pm 3} \mp \frac{1k}{2} D_{x_1}\phi_{11}^{\mp 1} \quad (z = -h), \tag{6.10}$$

where $\phi_{31}^{\pm 1}$ is denoted by f. The condition for this inhomogeneous problem to be solvable yields two coupled evolution equations for A and B, which can be combined with (2.53 a, b) to yield

$$\begin{pmatrix} A \\ B \end{pmatrix}_{t_1} \pm C_g \begin{pmatrix} A \\ B \end{pmatrix}_{x_1} + i\Omega_0 \begin{pmatrix} B \\ A \end{pmatrix} = \epsilon \left[ip \begin{pmatrix} A \\ B \end{pmatrix}_{x_1 x_1} \mp q \begin{pmatrix} B \\ A \end{pmatrix}_{x_1} + ir \begin{pmatrix} A \\ B \end{pmatrix} \mp s \begin{pmatrix} B \\ A \end{pmatrix} \right], \tag{6.11 $\frac{a}{b}$}$$

where

$$\left.\begin{aligned} p &= \frac{1}{2}\frac{\mathrm{d}^2\omega}{\mathrm{d}k^2}, \quad q = \frac{2\Omega_0 \sinh^2 kh}{k}, \\ r &= \frac{\Omega_0^2}{2\omega}\left(1 + 4\sinh^2 kh + 6\sinh 2kh \frac{\cosh 4kh + 2\cosh 2kh}{\sinh 4kh + 2\sinh 2kh}\right) \\ s &= \frac{gk}{4\omega} D_{x_1}. \end{aligned}\right\} \tag{6.12}$$

These are linear Schrödinger equations coupling A and B and are valid for $(x_2, t_2) = \epsilon(x_1, t_1) = O(1)$.

Let the solution be of the following form:

$$\begin{pmatrix} A \\ B \end{pmatrix} = \left[\begin{pmatrix} A_1 \\ B_1 \end{pmatrix} + \epsilon \begin{pmatrix} A_2 \\ B_2 \end{pmatrix} + \ldots \right] \mathrm{e}^{-i\Omega t_1}. \tag{6.13}$$

To the leading order the general solution is easily found to be

$$\left.\begin{aligned} A_1 &= A^+ \mathrm{e}^{\alpha_1 x_1} + A^- \mathrm{e}^{-\alpha_1 x_1}, \\ B_1 &= R^+ A^+ \mathrm{e}^{\alpha_1 x_1} + R^- A^- \mathrm{e}^{-\alpha_1 x_1}, \end{aligned}\right\} \tag{6.14}$$

with

$$\left.\begin{aligned} A^\pm &= A^\pm(x_2), \\ \alpha_1 &= \frac{\Omega_0}{C_g}\left(1 - \left(\frac{\Omega}{\Omega_0}\right)^2\right)^{\frac{1}{2}}, \quad R^\pm = \frac{\Omega}{\Omega_0} \pm i\left(1 - \left(\frac{\Omega}{\Omega_0}\right)^2\right)^{\frac{1}{2}} \quad \text{if } 1 > \left(\frac{\Omega}{\Omega_0}\right)^2, \\ \alpha_1 &= i\frac{\Omega_0}{C_g}\left(\left(\frac{\Omega}{\Omega_0}\right)^2 - 1\right)^{\frac{1}{2}}, \quad R^\pm = \frac{\Omega}{\Omega_0} \mp \left(\left(\frac{\Omega}{\Omega_0}\right)^2 - 1\right)^{\frac{1}{2}} \quad \text{if } \left(\frac{\Omega}{\Omega_0}\right)^2 > 1. \end{aligned}\right\} \tag{6.15}$$

The amplitudes $A^\pm$ are yet to be determined. We now substitute these results into (6.11 a, b) and eliminate B_2:

$$A_{2x_1x_1} - \alpha_1^2 A_2 = \frac{i\Omega_0}{C_g^2}\mathrm{e}^{\alpha_1 x_1}[C_g(R^+ - R^-)A_{x_2}^+ + ip\alpha_1^2(R^+ + R^-)A^+ + ir(R^+ + R^-)A^+]$$

$$+ \frac{i\Omega_0}{C_g^2}\mathrm{e}^{-\alpha_1 x_1}[-C_g(R^+ - R^-)A_{x_2}^- + ip\alpha_1^2(R^+ + R^-)A^- + ir(R^+ + R^-)A^-]. \tag{6.16}$$

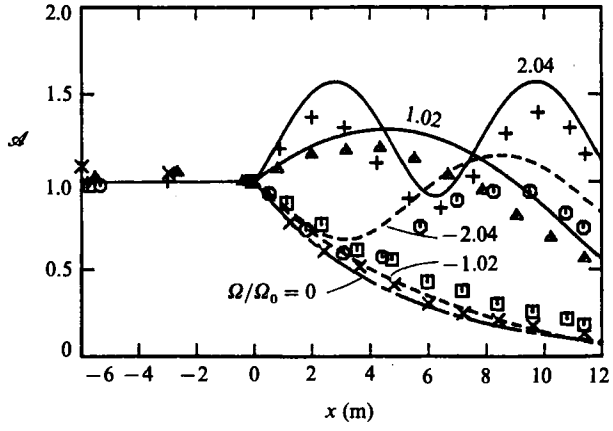

FIGURE 7. Wave height distribution at antinodes (higher order approximation): +, $\Omega/\Omega_0 = 2.04$; △, 1.02; ×, 0; □, −1.02; ○, −2.04. Theoretical solutions are shown by curves: numbers by the curves give Ω/Ω_0.

Since $\exp(\pm\alpha_1 x_1)$ are homogeneous solutions of the differential equation, we must insist that their coefficients on the right-hand side vanish to avoid unboundedness as $x_1 \to \infty$ or $x_2 = O(1)$. This gives

$$\pm C_g(R^+ - R^-)A^\pm_{x_2} + ip\alpha_1^2(R^+ + R^-)A^\pm + ir(R^+ + R^-)A^\pm = 0, \tag{6.17}$$

which implies

$$A^\pm = a^\pm \exp(\pm\alpha_2 x_2), \tag{6.18}$$

with

$$\alpha_2 = -i(p\alpha_1^2 + r)\frac{1}{C_g}\frac{R^+ + R^-}{R^+ - R^-}. \tag{6.19}$$

We now summarize the first-order solution valid for $x_2 = O(1)$:

$$\left.\begin{aligned} A &= a^+ e^{\alpha_1 x_1 + \alpha_2 x_2} + a^- e^{-(\alpha_1 x_1 + \alpha_2 x_2)}, \\ B &= R^+ a^+ e^{\alpha_1 x_1 + \alpha_2 x_2} + R^- a^- e^{-(\alpha_1 x_1 + \alpha_2 x_2)}. \end{aligned}\right\} \tag{6.20}$$

To determine the coefficients $a^\pm$ we apply the boundary condition (4.6) at $x = L$ (or $x_2 = L_2$), with the result

$$a^- = Z_1 a^+, \quad Z_1 = -\frac{1 - iR^+}{1 - iR^-} e^{2(\alpha_1 L_1 + \alpha_2 L_2)}, \tag{6.21}$$

which implies

$$A(x) = a^+[e^{\alpha_1 x_1 + \alpha_2 x_2} + Z_1 e^{-(\alpha_1 x_1 + \alpha_2 x_2)}], \tag{6.22a}$$

$$B(x) = a^+[R^+ e^{\alpha_1 x_1 + \alpha_2 x_2} + Z_1 R^- e^{-(\alpha_1 x_1 + \alpha_2 x_2)}]. \tag{6.22b}$$

From here we can omit the distinction between x_1 and x_2 and set $\epsilon = 1$.

To determine the coefficient a^+ completely one must in principle solve for the corresponding A and B in the barless region between the wavemaker and the edge at $x = 0$. This would involve the solution of a set of equations which are uncoupled because $\Omega_0 = q = r = s = 0$, but with variable coefficients because of the changing depth. Furthermore the kinematic boundary condition at the wavemaker must be satisfied. This is complicated and not relevant here. We therefore choose to study

the ratio of the envelope height at the antinodes in the strip to the envelope height at the edge of the strip, i.e.

$$\mathscr{A}(x) = \frac{|A(x)|+|B(x)|}{|A(0)|+|B(0)|} \quad (0 < x < L) \tag{6.23}$$

where A and B are given by (6.22a, b).

The ratio $\mathscr{A}(x)$ is compared to the measured data in figure 7 and the agreement for all cases in which $(\Omega/\Omega_0)^2$ differs from unity is remarkable. Thus we have established the existence and the physical properties of Ω_0 although the quantitative confirmation requires a higher-order theory.

We point out that by setting $\alpha_2 = 0$ in (6.22) the result is the crudest approximation which did not compare well with the experiments.

If $(\Omega/\Omega_0)^2 = 1$, $\alpha_1 = R^+ - R^- = 0$, $\alpha_2 \to \infty$, (6.22) breaks down. The assumed perturbation expansion (6.13) must be modified. The analysis is slightly more involved and is described in the Appendix. The results are given by (A 28a, b). The ratio $\mathscr{A}(x)$ is plotted in figure 7 for $\Omega = \pm\Omega_0$. Again they agree quite well with the experiments.

7. Concluding remarks

From the experiments and the corresponding theory described in this paper, certain physical characteristics of Bragg resonance of surface waves have been established. In the case of a uniform wavetrain, there is a cutoff frequency for detuning frequencies. For Ω above the cutoff the envelope oscillates in x; for Ω below the cutoff, the envelope is monotonic. For wave packets the wave envelope is dispersive, and two kinds of long waves can be radiated.

For moderately large amplitude it is of scientific interest to study the initial instability and the subsequent nonlinear evolution of narrow-banded waves over sandbars; this and other aspects must await future studies of the coupled cubic Schrödinger equations extended from (6.11a, b).

For this study we have received financial support from the US Office of Naval Research (Contract N00014-83K-0550) and the US National Science Foundation (Grant 8210649). T. Hara also thanks the Japanese Ministry of Education for a Fellowship during 1984–1985.

Appendix. Higher-order theory for the critical case of $\Omega/\Omega_0 = \pm 1$

For the strip $0 < x < L$ we begin by assuming

$$\begin{pmatrix} A \\ B \end{pmatrix} = \begin{pmatrix} \overline{A} \\ \overline{B} \end{pmatrix} e^{-i\Omega t_1} \tag{A 1}$$

and then eliminating $\overline{B}$ from (6.11a, b) by cross-differentiation, yielding

$$-C_g \frac{d^2\overline{A}}{dx_1^2} = \epsilon\{+2\Omega r\overline{A} + 2\Omega p\overline{A}_{x_1 x_1}\} + O(\epsilon^2) \tag{A 2}$$

for D = constant. $\overline{B}$ satisfies the same equation. From (A 2) we find a new balance between the left-hand side and the first term on the right, if the x-coordinate is rescaled by

$$\overline{x} = \epsilon^{\frac{1}{2}} x_1 = \epsilon^{\frac{1}{2}} x. \tag{A 3}$$

Now we rewrite (6.11a, b), after using (A 1),

$$-\mathrm{i}\Omega\begin{pmatrix}\overline{A}\\ \overline{B}\end{pmatrix}\pm\epsilon^{\frac{1}{2}}C_{\mathrm{g}}\begin{pmatrix}\overline{A}\\ \overline{B}\end{pmatrix}_{\bar{x}}+\mathrm{i}\Omega_0\begin{pmatrix}\overline{B}\\ \overline{A}\end{pmatrix}=\epsilon ir\begin{pmatrix}\overline{A}\\ \overline{B}\end{pmatrix}\mp\epsilon^{\frac{3}{2}}q\begin{pmatrix}\overline{B}\\ \overline{A}\end{pmatrix}_{\bar{x}}+\epsilon^2 ip\begin{pmatrix}\overline{A}\\ \overline{B}\end{pmatrix}_{\bar{x}\bar{x}}. \tag{A 4}$$

Let us assume the solutions to be the following expansions:

$$\begin{pmatrix}\overline{A}\\ \overline{B}\end{pmatrix}=\begin{pmatrix}A_0\\ B_0\end{pmatrix}+\epsilon^{\frac{1}{2}}\begin{pmatrix}A_{\frac{1}{2}}\\ B_{\frac{1}{2}}\end{pmatrix}+\epsilon\begin{pmatrix}A_1\\ B_1\end{pmatrix}+\epsilon^{\frac{3}{2}}\begin{pmatrix}A_{\frac{3}{2}}\\ B_{\frac{3}{2}}\end{pmatrix}+\ldots, \tag{A 5}$$

of which the first two terms will be used in the computations. Substitution of (A 5) into (A 4) yields a sequence of perturbation equations,

$O(\epsilon^0)$:

$$-\mathrm{i}\Omega\begin{pmatrix}A_0\\ B_0\end{pmatrix}+\mathrm{i}\Omega_0\begin{pmatrix}B_0\\ A_0\end{pmatrix}=0, \tag{A 6$\frac{a}{b}$}$$

$O(\epsilon^{\frac{1}{2}})$:

$$-\mathrm{i}\Omega\begin{pmatrix}A_{\frac{1}{2}}\\ B_{\frac{1}{2}}\end{pmatrix}+\mathrm{i}\Omega_0\begin{pmatrix}B_{\frac{1}{2}}\\ A_{\frac{1}{2}}\end{pmatrix}\pm C_{\mathrm{g}}\begin{pmatrix}A_0'\\ B_0'\end{pmatrix}=0, \tag{A 7$\frac{a}{b}$}$$

$O(\epsilon^1)$:

$$-\mathrm{i}\Omega\begin{pmatrix}A_1\\ B_1\end{pmatrix}+\mathrm{i}\Omega_0\begin{pmatrix}B_1\\ A_1\end{pmatrix}\pm C_{\mathrm{g}}\begin{pmatrix}A_{\frac{1}{2}}'\\ B_{\frac{1}{2}}'\end{pmatrix}=\mathrm{i}r\begin{pmatrix}A_0\\ B_0\end{pmatrix}, \tag{A 8$\frac{a}{b}$}$$

$O(\epsilon^{\frac{3}{2}})$:

$$-\mathrm{i}\Omega\begin{pmatrix}A_{\frac{3}{2}}\\ B_{\frac{3}{2}}\end{pmatrix}+\mathrm{i}\Omega_0\begin{pmatrix}B_{\frac{3}{2}}\\ A_{\frac{3}{2}}\end{pmatrix}\pm C_{\mathrm{g}}\begin{pmatrix}A_1'\\ B_1'\end{pmatrix}=\mathrm{i}r\begin{pmatrix}A_{\frac{1}{2}}\\ B_{\frac{1}{2}}\end{pmatrix}\mp q\begin{pmatrix}B_0'\\ A_0'\end{pmatrix}, \tag{A 9$\frac{a}{b}$}$$

where $(\ )' \equiv \mathrm{d}(\ )/\mathrm{d}\bar{x}$. Using the convention that the upper and lower signs correspond to $\Omega = +\Omega_0$ and $-\Omega_0$ respectively, we obtain from (A 6a, b) that

$$A_0 = \pm B_0. \tag{A 10}$$

By combining (A 7a, b) we get

$$\pm 2\mathrm{i}\Omega_0(A_{\frac{1}{2}}\mp B_{\frac{1}{2}}) = C_{\mathrm{g}}(A_0 \pm B_0)'. \tag{A 11}$$

Similarly from (A 8a, b) we get

$$C_{\mathrm{g}}(A_{\frac{1}{2}}'\mp B_{\frac{1}{2}}') = \mathrm{i}r(A_0 \pm B_0). \tag{A 12}$$

Elimination of $A_{\frac{1}{2}}$ and $B_{\frac{1}{2}}$ gives

$$(A_0 \pm B_0)'' \pm \frac{2r\Omega_0}{C_{\mathrm{g}}^2}(A_0 \pm B_0) = 0. \tag{A 13}$$

The solution is

$$A_0 = \pm B_0 = \tfrac{1}{2}(a_0^+ \,\mathrm{e}^{\alpha_3 \bar{x}} + a_0^- \,\mathrm{e}^{-\alpha_3 \bar{x}}) \tag{A 14}$$

where

$$\alpha_3 = \begin{pmatrix}\mathrm{i}\\ 1\end{pmatrix}\frac{(2r\Omega_0)^{\frac{1}{2}}}{C_{\mathrm{g}}} \quad \text{if } \Omega = \pm\Omega_0. \tag{A 15}$$

Equation (A 11) then gives

$$(A_{\frac{1}{2}}\mp B_{\frac{1}{2}}) = \pm\frac{C_{\mathrm{g}}\alpha_3}{2\mathrm{i}\Omega_0}(a_0^+ \,\mathrm{e}^{\alpha_3 \bar{x}} - a_0^- \,\mathrm{e}^{-\alpha_3 \bar{x}}). \tag{A 16}$$

We now eliminate A_0 and B_0 from (A 8a, b),

$$C_{\mathrm{g}}(A_{\frac{1}{2}} \pm B_{\frac{1}{2}})' = \pm 2\mathrm{i}\Omega_0(A_1 \mp B_1), \tag{A 17}$$

and similarly $A_{\frac{3}{2}}$ and $B_{\frac{3}{2}}$ from (A 9a, b),

$$C_g(A_1 \mp B_1)' = ir(A_{\frac{1}{2}} \pm B_{\frac{1}{2}}). \tag{A 18}$$

Equations (A 16)–(A 18) can be solved to obtain

$$\left.\begin{aligned} A_{\frac{1}{2}} &= a_{\frac{1}{2}}^+ \, e^{\alpha_3 \bar{x}} + a_{\frac{1}{2}}^- \, e^{-\alpha_3 \bar{x}}, \\ B_{\frac{1}{2}} &= \left(\pm a_{\frac{1}{2}}^+ - \frac{C_g \alpha_3}{2i\Omega_0} a_0^+ \right) e^{\alpha_3 \bar{x}} + \left(\pm a_{\frac{1}{2}}^- + \frac{C_g \alpha_3}{2i\Omega_0} a_0^- \right) e^{-\alpha_3 \bar{x}}. \end{aligned}\right\} \tag{A 19}$$

The constants $a_0^\pm$ and $a_{\frac{1}{2}}^\pm$ remain to be determined by the boundary conditions. At the vertical wall, condition (4.6) gives

$$a_0^- = Z_1 a_0^+ \quad \text{with } Z_1 = -e^{2\alpha_3 L} \tag{A 20}$$

at $O(\epsilon^0)$, and

$$Z_3 a_{\frac{1}{2}}^+ + Z_4 a_{\frac{1}{2}}^- = Z_5 a_0^+ \tag{A 21}$$

at $O(\epsilon^{\frac{1}{2}})$, with

$$Z_3 = e^{\alpha_3 L}(1 \mp i), \quad Z_4 = e^{-\alpha_3 L}(1 \mp i), \tag{A 21a, b}$$

$$Z_5 = \frac{C_g \alpha_3}{2\Omega_0}(-e^{\alpha_3 L} + Z_1 e^{-\alpha_3 L}). \tag{A 21c}$$

If we neglect the $O(\epsilon^{\frac{1}{2}})$ term we can stop here as in §6, but the accuracy cannot be very good. In order to solve for $a_{\frac{1}{2}}^\pm$ we need the solution in the region between the bars and the wavemaker ($x = -x_0$). As far as the bars are concerned, the refraction effect of changing depth can be approximately accounted for by considering an equivalent tank with constant depth everywhere between the bars and the wavemaker but with the horizontal length x_0 shortened so that the number of waves between them is the same. Specifically the actual distance is 9.09 m but the adjusted distance in the equivalent tank is $x_0 = 8.85$ m. Now we set $\Omega_0 = q = r = s = 0$ in (6.11a, b); A and B are now uncoupled. It is easy to derive from the reduced equations that

$$\begin{aligned} A &= (A_0^1 + \epsilon^{\frac{1}{2}} A_{\frac{1}{2}}^1 + \ldots) \, e^{\mp i\Omega_0 t} \\ &= (a_0^1 + \epsilon^{\frac{1}{2}} a_{\frac{1}{2}}^1 + \ldots) \exp\left(\pm i \frac{\Omega_0 X_1}{C_g} \right) \exp(\mp i\Omega_0 t), \end{aligned} \tag{A 22a}$$

$$\begin{aligned} B &= (B_0^1 + \epsilon^{\frac{1}{2}} B_{\frac{1}{2}}^1 + \ldots) \, e^{\mp i\Omega_0 t} \\ &= (b_0^1 + \epsilon^{\frac{1}{2}} b_{\frac{1}{2}}^1 + \ldots) \exp\left(\mp i \frac{\Omega_0 x_1}{C_g} \right) \exp(\mp i\Omega_0 t). \end{aligned} \tag{A 22b}$$

Matching of A and B at $x = 0$ gives

$$\tfrac{1}{2}(a_0^+ + a_0^-) = a_0^1, \quad \pm\tfrac{1}{2}(a_0^+ + a_0^-) = b_0^1 \tag{A 23a, b}$$

at $O(\epsilon^0)$, and

$$a_{\frac{1}{2}}^+ + a_{\frac{1}{2}}^- = a_{\frac{1}{2}}^1, \quad \pm a_{\frac{1}{2}}^+ - \frac{C_g \alpha_3}{2i\Omega_0} a_0^+ \pm a_{\frac{1}{2}}^- + \frac{C_g \alpha_3}{2i\Omega_0} a_0^- = b_{\frac{1}{2}}^1 \tag{A 24a, b}$$

at $O(\epsilon^{\frac{1}{2}})$. Finally the boundary conditions at the equivalent wavemaker is

$$\phi_{11x} = -i\omega\xi_{11},$$

where ξ_{11} is the horizontal displacement of the wavemaker. This implies at $O(\epsilon^0)$

$$A_0^1 \, e^{i(-kx_0 - \frac{1}{4}\pi)} - B_0^1 \, e^{i(kx_0 + \frac{1}{4}\pi)} = N\xi_{11}, \tag{A 25}$$

where

$$N = \frac{-\mathrm{i}\omega \int_{-h}^{0} f_0 \,\mathrm{d}z}{\mathrm{i}k \int_{-h}^{0} f_0^2 \,\mathrm{d}z}, \quad f_0 = -\frac{\mathrm{i}g}{2\omega} \frac{\cosh k(z+h)}{\cosh kh}, \tag{A 26}$$

and at $O(\epsilon^{\frac{1}{2}})$

$$A_{\frac{1}{2}}^1 \,\mathrm{e}^{\mathrm{i}(-kx_0 - \frac{1}{4}\pi)} - B_{\frac{1}{2}}^1 \,\mathrm{e}^{\mathrm{i}(kx_0 + \frac{1}{4}\pi)} = 0, \tag{A 27}$$

where A_0^1, B_0^1, $A_{\frac{1}{2}}^1$ and $B_{\frac{1}{2}}^1$ are related to a_0^1, b_0^1, $a_{\frac{1}{2}}^1$ and $b_{\frac{1}{2}}^1$ by (A 22a, b). From (A 20), (A 23a, b) and (A 25) we solve for $a_0^{\pm}$, a_0^1, b_0^1, while from (A 21), (A 24a, b) and (A 27) we solve for $a_{\frac{1}{2}}^{\pm}$, $a_{\frac{1}{2}}^1$ and $b_{\frac{1}{2}}^1$:

$$A = \frac{N}{Z_2} \xi_{11} \left[\mathrm{e}^{\alpha_3 \bar{x}} \left(\tfrac{1}{2} + \epsilon^{\frac{1}{2}} \frac{Z_5 Z_6 - Z_4 Z_7}{Z_6(Z_3 - Z_4)} \right) + \mathrm{e}^{-\alpha_3 \bar{x}} \left(\frac{Z_1}{2} - \epsilon^{\frac{1}{2}} \frac{Z_5 Z_6 - Z_3 Z_7}{Z_6(Z_3 - Z_4)} \right) \right], \tag{A 28a}$$

$$B = \frac{N}{Z_2} \xi_{11} \left\{ \mathrm{e}^{\alpha_3 \bar{x}} \left[\pm \tfrac{1}{2} + \epsilon^{\frac{1}{2}} \left(\pm \frac{Z_6 Z_5 - Z_4 Z_7}{Z_6(Z_3 - Z_4)} - \frac{C_g}{2\mathrm{i}\Omega_0} \alpha_3 \right) \right] \right.$$
$$\left. + \mathrm{e}^{-\alpha_3 \bar{x}} \left[\pm \frac{Z_1}{2} + \epsilon^{\frac{1}{2}} \left(\pm \frac{-Z_6 Z_5 + Z_3 Z_7}{Z_6(Z_3 - Z_4)} + \frac{C_g}{2\mathrm{i}\Omega_0} \alpha_3 Z_1 \right) \right] \right\}, \tag{A 28b}$$

with

$$Z_2 = \tfrac{1}{2}(1 + Z_1) \exp\left[\mp \frac{\mathrm{i}\Omega_0}{C_g} x_0 + \mathrm{i}(-kx_0 - \tfrac{1}{4}\pi) \right] \mp \tfrac{1}{2}(1 + Z_1) \exp\left[\pm \frac{\mathrm{i}\Omega_0}{C_g} x_0 - \mathrm{i}(-kx_0 - \tfrac{1}{4}\pi) \right], \tag{A 28c}$$

$$Z_6 = \exp\left[\mp \frac{\mathrm{i}\Omega_0}{C_g} x_0 \right] \mp \exp\left[\pm \frac{\mathrm{i}\Omega_0}{C_g} x_0 + 2\mathrm{i}kx_0 \right], \tag{A 28d}$$

$$Z_7 = \frac{C_g}{2\Omega_0} \alpha_3 (Z_1 - 1) \exp\left[\pm \frac{\mathrm{i}\Omega_0}{C_g} x_0 + 2\mathrm{i}kx_0 \right]. \tag{A 28e}$$

Again the ratio

$$\mathscr{A}(x) = \frac{|A(x)| + |B(x)|}{|A(0)| + |B(0)|} \tag{A 29}$$

is plotted, which is independent of ξ_{11}.

REFERENCES

Davies, A. G. 1982 The reflection of wave energy by undulations on the seabed. *Dyn. Atmos. Oceans* **6**, 207–232.

Davies, A. G. & Heathershaw, A. D. 1984 Surface-wave propagation over sinusoidally varying topography. *J. Fluid Mech.* **144**, 419–443.

Hara, T. 1985 Resonant reflection of water waves by periodic sandbars. Masters thesis, Department of Civil Engineering, University of Tokyo.

Heathershaw, A. D. 1982 Seabed-wave resonance and sandbar growth. *Nature* **296**, 343–345.

Hunt, J. N. 1952 Viscous damping of waves over an inclined bed in a channel of finite width. *Houille Blanche* **7**, 836–842.

Mei, C. C. 1985 Resonant reflection of surface water waves by periodic sandbars. *J. Fluid Mech.* **152**, 315–335.